Supplementary Information for

On-site portable detection of gaseous I_2 using green and pollution-free electrochemical methods

Xiao-Lan Yang, Qiu-Hong Zhu, Guo-Hao Zhang, Shuang-Long Wang, Lijian Ma, Song Qin, Guo-Hong Tao*, Ling He*

College of Chemistry, Sichuan University, Chengdu, Sichuan 610064, China.

E-mail: lhe@scu.edu.cn.

E-mail: taogh@scu.edu.cn.

Table of Contents

Experimental Section

Materials

In this work, both monomer 1-vinylimidazole (VIm, 98%) and initiator 2,2′-azobis(2-methylpropionitrile) (AIBN, 99%) were obtained from Energy Chemical. Bromoethane (C_2H_5Br, 98%) and other reagents were purchased from Leyan. All the solvents involved in the experiments and reagents above were analytical grade and without further purification. Ultrapure water of 18.25 MΩ cm was used throughout the entire experiment.

Synthesis of PIL

VIm was polymerized to PVIm by free radical polymerization reaction using 10 wt% AIBN as initiator. According to the literature[1], C_2H_5Br and PVIm (the molar ratio of VIm monomer to C_2H_5Br was 1:2) were reacted in anhydrous ethanol for two days at 50 °C. After that, ethyl acetate was used to precipitate the solid crude product, and finally the crude product was dried under vacuum at 70 °C for 48 h to obtain a white poly(1-vinyl-3-ethylimidazolium bromide). The synthesized solid powder was named as PIL with a yield of 90%.

The signal peaks at the low field of 6.69-9.71 ppm represent the three protons on the imidazole ring (H3, H4, and H5). In addition to solvent peaks between 1.18-1.44 ppm, there are also two proton peaks belonging to the main chain -CH_2- structure. Due to the hydrophilicity of imidazole group, the proton peaks of CH group on the main chain coincide with the H_2O peak, appearing around 3.41 ppm. Besides, the proton peaks of C_2H_5- attached to N^+ appeared at 1.91-2.71 ppm (H7) and 4.02-4.19 ppm (H6), respectively.

The results of ^{13}C NMR correspond to those of ^{1}H NMR: the chemical shifts of C1 on the main chain and C7 on the branch chain appear at 14.87 ppm, C2 on the main chain at 40.98 ppm, C6 on the branched chain at 46.36 ppm, and C3, C4, and C5 on the imidazole ring appeared between 118.88-138.53 ppm.

Synthesis of PIL-film

The PIL-film was prepared as follows: a certain amount of PIL was dissolved in a test tube containing anhydrous ethanol, and allowed it to dissolve fully into a homogeneous solution. The solution was then poured into a mold to form a film by

solvent evaporation at room temperature for 48 hours. The as-prepared film was named PIL-film.

Material characterization

The NMR spectra of PIL were recorded by a Bruker 400 MHz nuclear magnetic resonance (NMR) spectrometer (Germany). The ^{1}H NMR of PIL was probed with DMSO d_6 as the locking solvent, and the ^{13}C NMR was probed with methanol-d_4 as the locking solvent. Fourier transform infrared (FT-IR) spectra in the range of 400-4000 cm^{-1} were recorded using a Bruker ALPHA (Germany) infrared spectrometer. The transmittances of PIL-film were characterized by scanning the wavelength from 400 to 800 nm using an ultraviolet visible spectrophotometer (Rayleigh UV-1601). Contact angle (CA) images were recorded on the ZHONGCHEN JC2000DS (China) contact angle measuring instrument, which equipped with a CCD camera. The digital photograph of PIL-film was recorded with a Redmi K40. The zeta potential of the films at 298 k were determined by Zetasizer Nano ZS90 DLS spectrometer (Malvern Inc., UK), and the pH of the systems were controlled between 3-11 by 0.01 mol/L NaOH and 0.01 mol/L HCl solutions. For the thermal properties, the glass transition temperature (T_g) of the sample was determined by a TA Q20 differential scanning calorimeter (DSC) at a N_2 flow rate of 50 mL/min and a scan rate of 10 °C/min, where an empty aluminum container was the reference sample. And the decomposition temperature (T_d) of the sample was determined by a thermogravimetric analysis (TGA, NETZSCH TG209F1), where the tests were performed at 10 °C/min from ambient temperature to 800 °C. The structures of the samples were analyzed by X-ray photoelectron spectroscopy (XPS, Thermo Scientific K-Alpha+). The Raman spectrum was obtained using a RenishawinVia equipped with a 532 nm diode laser.

Electrochemical tests

The working electrode and counter electrode of the screen-printing electrode are carbon electrodes, and the reference electrode is Ag/AgCl electrode. By using the drop casting method, PIL was uniformly dropped onto the grooves of the screen-printing electrode to form a film (PIL-film). After inserting it into the corresponding electrode

adapter, cyclic voltammetry (CV) testing was performed on the Autolab M204 electrochemical workstation to obtain the concentration of I_2 vapor based on the intensity of the I_2 redox peaks.

The physical and chemical properties of various iodine nuclides are similar[2], and the I_2 vapor used in this work was obtained by heating the stable $^{127}I_2$. Putted solid I_2 into a closed container and heated it at 75 °C to rapidly sublimate. When the system was stabilized, allow the sensor composed of PIL-film and screen-printing electrodes to come into contact with I_2 vapor. Unless otherwise specified, each experiment was tested 5 times in parallel to ensure the reproducibility of the experimental results. The test device diagram is shown in **Fig. S1**.

Fig. S1. The device diagram of electrochemical detection.

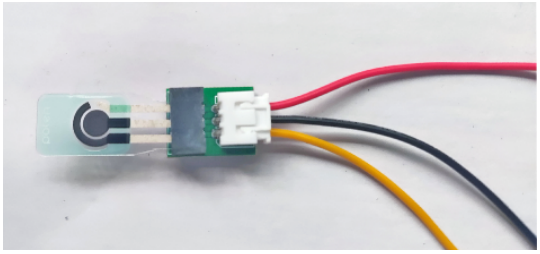

Theoretical calculations

Based on the density functional theory (DFT) and Gaussian 09 (Revision A.02) suite of programs, the dimer model of PIL was subjected to structural optimization in the gas phase at the B3LYP-D3/def2TZVP level[3]. The frequency calculation for structural optimization did not show any imaginary frequencies, indicating that its geometric energies was at the minimum value. The Gaussian output .fch file was further used as the input file for Multiwfn, and then the quantitative analysis of molecular surface electrostatic potential distribution (ESP) was carried out[4]. Finally, the molecular ESP mapping isosurface was obtained through VMD 1.9.3[5].

Results and Discussion

Fig. S2. The ^{1}H NMR of PIL.

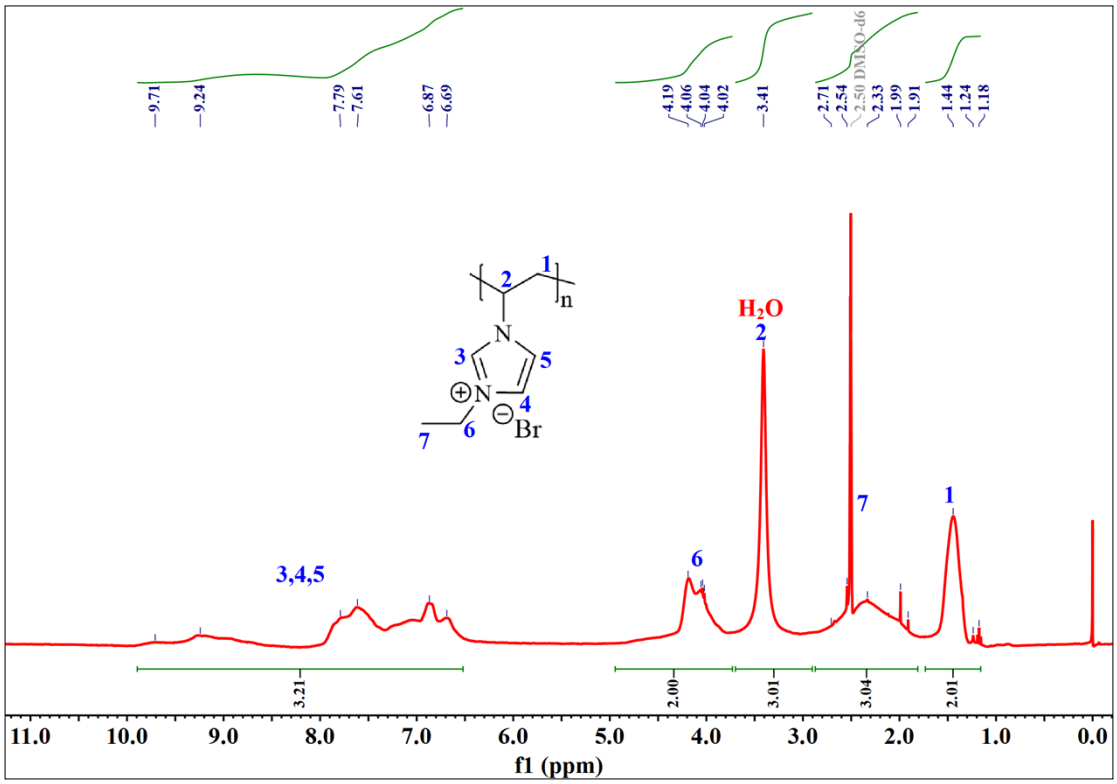

Fig. S3. The ^{13}C NMR of PIL.

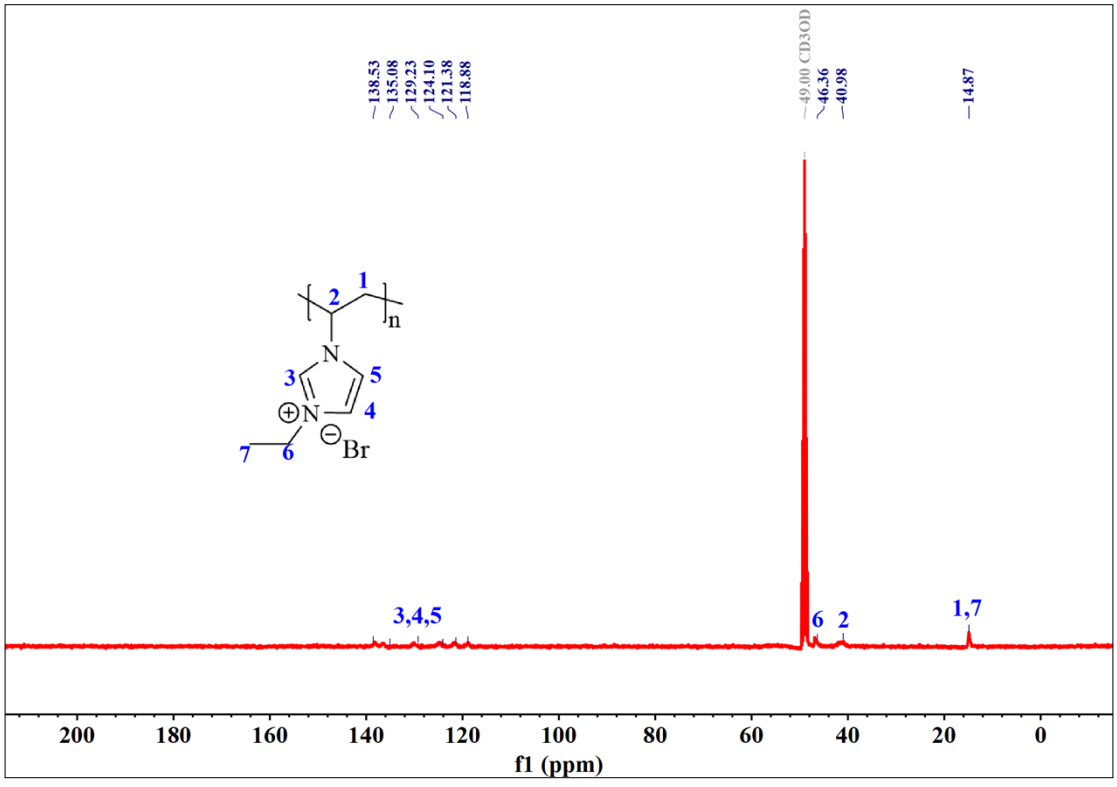

Fig. S4. The FT-IR spectra of PIL and PIL-film.

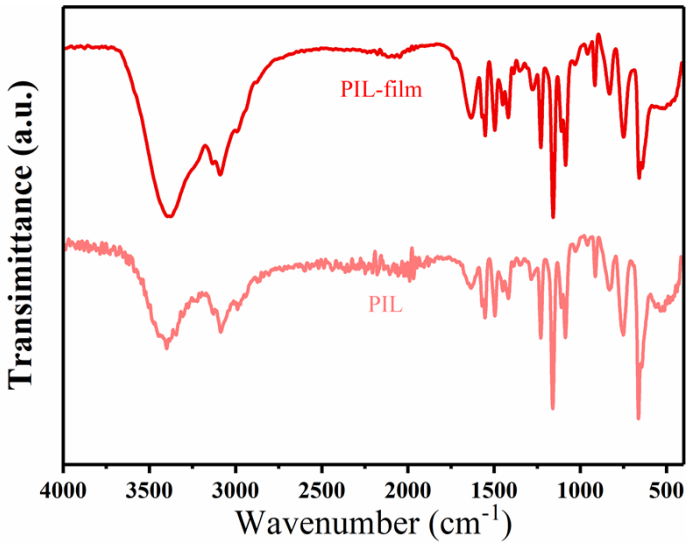

Fig. S5. The pictures of contact angle of PVIm-film and PIL-film over time.

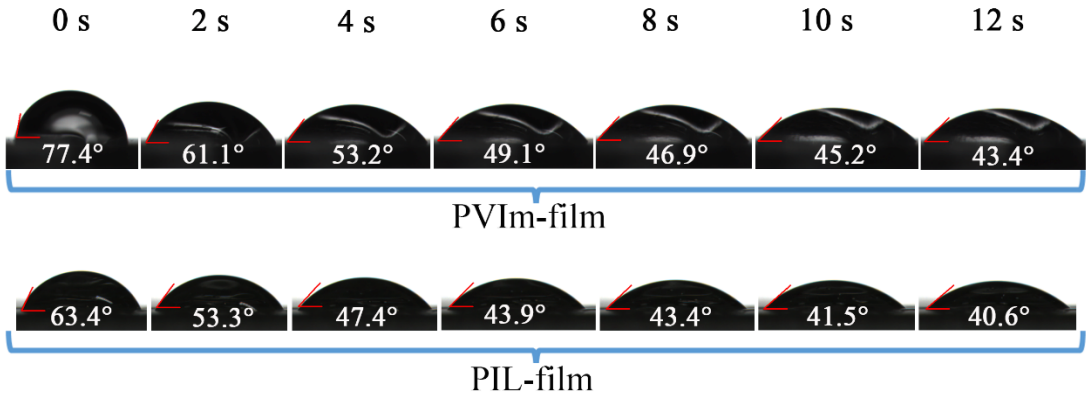

Fig. S6. The CV curves of the PIL-film based sensor at different scanning rates.

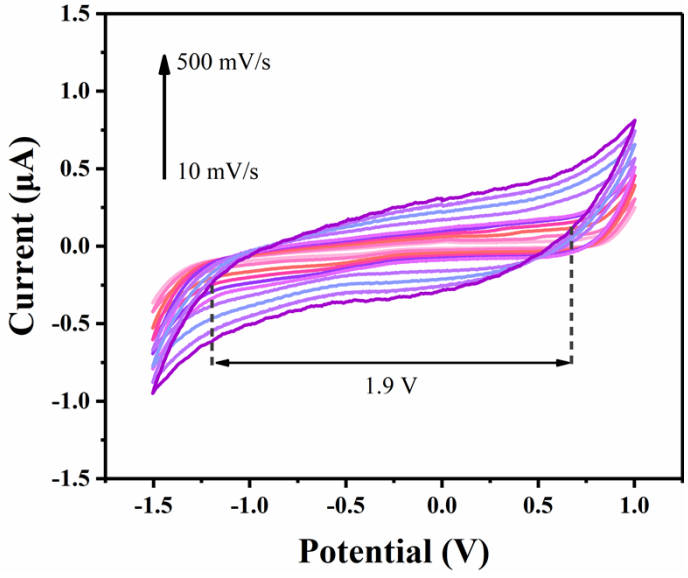

Fig. S7. The CV curves of PIL-film based sensor after different time of I_2 enrichment.

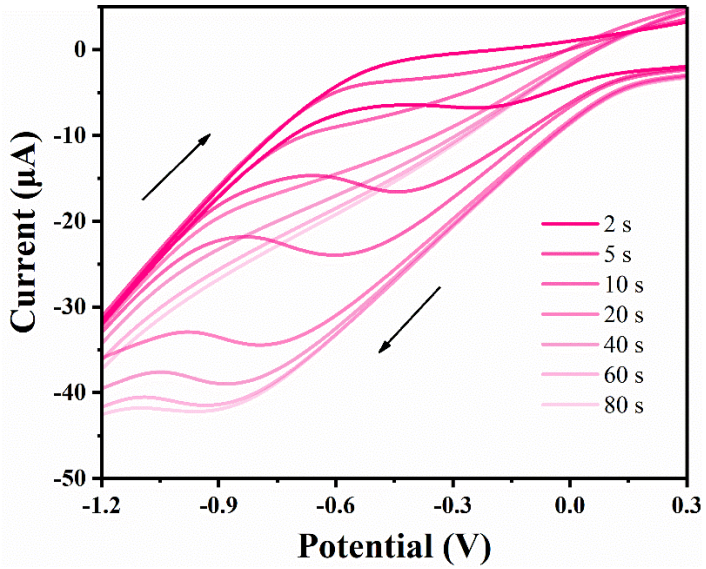

Fig. S8. The curve of reduction peak current values with different enrichment time.

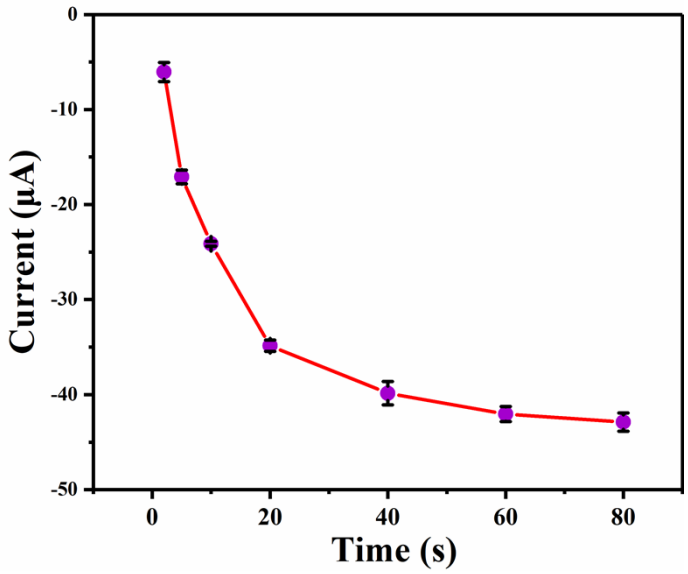

Table. S1. The summary of detection limits previously reported in this field.

Serial no.	Materials	Detection method	Time	LOD	Ref.
1	IOW-ATR	UV-Vis	15 s	4 ppm	6
2	PIM-1	FS	30 s	20 ppb	7
3	CMPN@FP	FS	5 min	24 μg/L	8
4	IPIN	CV DPV	80 S	0.047 μM 5.881 nM	9
5	PIL-film	CV	60 s	1.44 nM	This work

Fig. S9. The I_2 selectivity of the PIL-film based sensor.

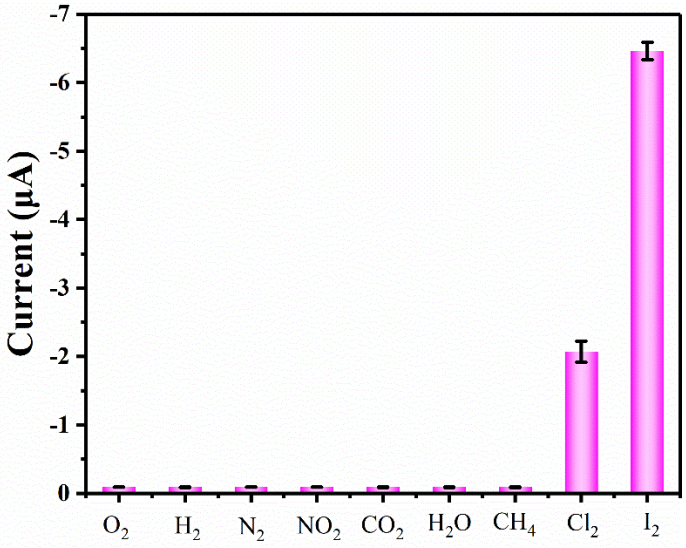

Fig. S10. XPS full survey spectra of PIL-film and PIL-film with I_2.

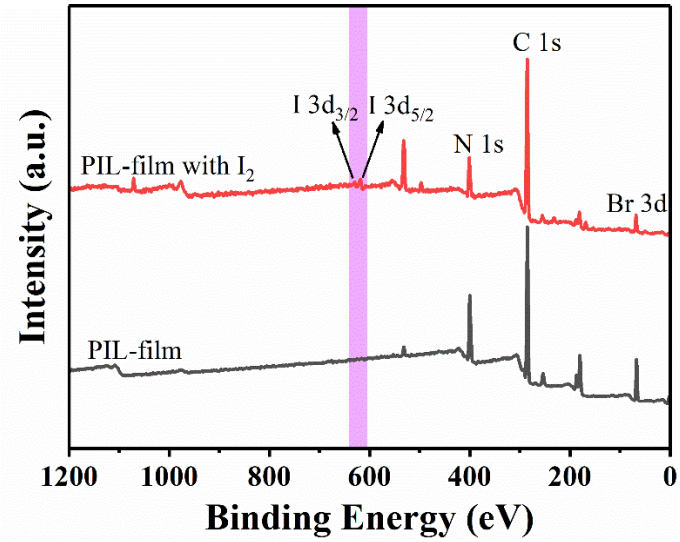

Fig. S11. N 1s XPS spectra of PIL-film and PIL-film with I_2.

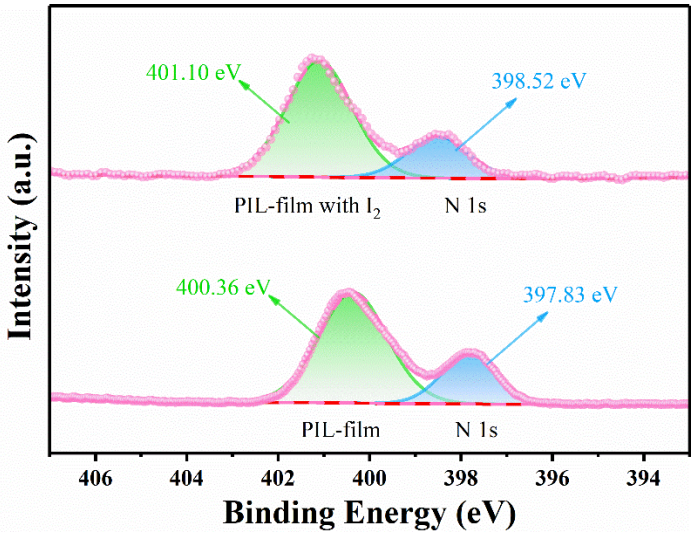

Fig. S12. ESP-mapped molecular surface area.

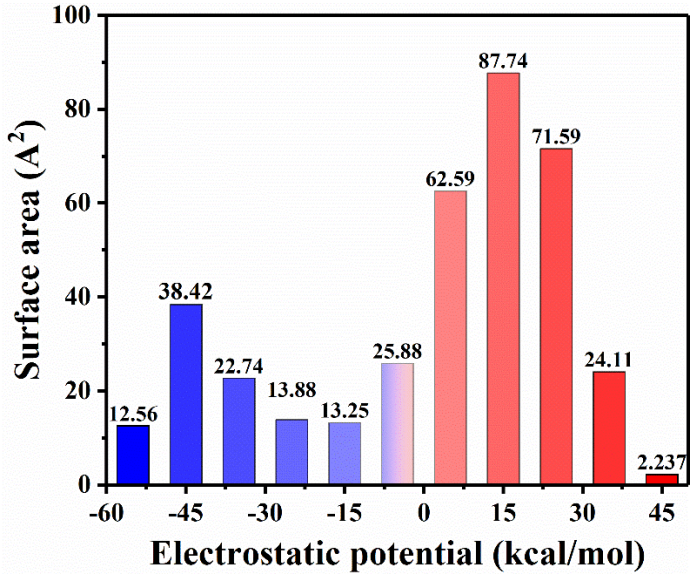

Fig. S13. The (a) storage and (b) reusable performance of sensors based on PIL-film.

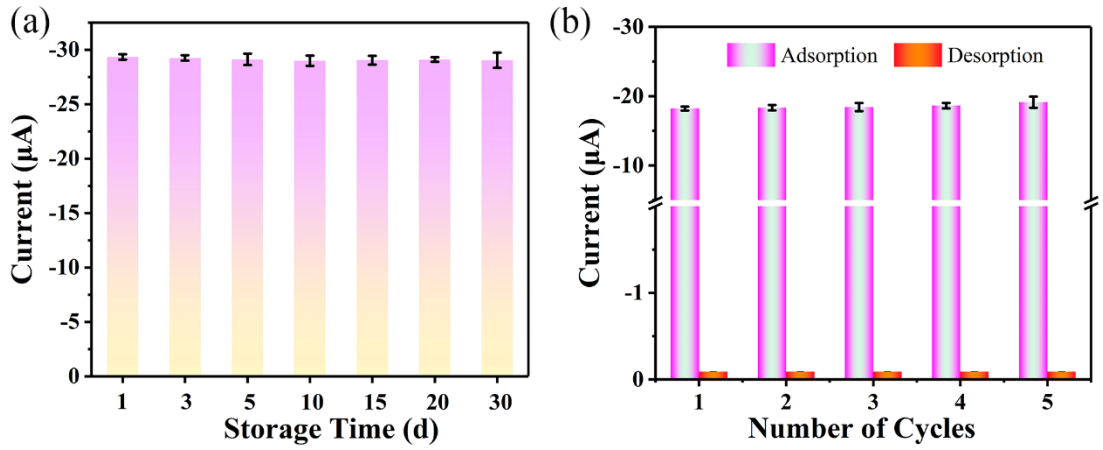

Table. S2. The cost of the currently reported I_2 detection materials.

Serial no.	Materials	Costing/Price	Ref.
1	PIM-1	12.6 $/g	7
2	CMPN@FP	38.3 $/g	8
3	IPIN	4.7 $/g	9
4	PIL-film	0.13 ¢ /piece or 15 ¢ /g	This work

References

1 K. Yin, Z. Zhang, L. Yang and S. I. Hirano, *J. Power Sources*, 2014, **258**, 150-154.

2 A. Bo, S. Sarina, Z. Zheng, D. Yang, H. Liu and H. Zhu, *J. Hazard. Mater.*, 2013, **246-247**, 199-205.

3 M. J. Frisch, G. W. Trucks, H. B. Schlegel, G. E. Scuseria, M. A. Robb, J. R. Cheeseman, G. Scalmani, V. Barone, B. Mennucci, G. A. Petersson, H. Nakatsuji, M. Caricato, X. Li, H. P. Hratchian, A. F. Izmaylov, J. Bloino, G. Zheng, J. L. Sonnenberg, M. Hada, M. Ehara, K. Toyota, R. Fukuda, J. Hasegawa, M. Ishida, T. Nakajima, Y. Honda, O. Kitao, H. Nakai, T. Vreven, J. A. Montgomery, J. E. P. Jr., F. Ogliaro, M. Bearpark, J. J. Heyd, E. Brothers, K. N. Kudin, V. N. Staroverov, R. Kobayashi, J. Normand, K. Raghavachari, A. Rendell, J. C. Burant, S. S. Iyengar, J. Tomasi, M. Cossi, N. Rega, J. M. Millam, M. Klene, J. E. Knox, J. B. Cross, V. Bakken, C. Adamo, J. Jaramillo, R. Gomperts, R. E. Stratmann, O. Yazyev, A. J. Austin, R. Cammi, C. Pomelli, J. W. Ochterski, R. L. Martin, K. Morokuma, V. G. Zakrzewski, G. A. Voth, P. Salvador, J. J. Dannenberg, S. Dapprich, A. D. Daniels, O. Farkas, J. B. Foresman, J. V. Ortiz, J. Cioslowski and D. J. Fox, Gaussian 09, Revision D.01. Gaussian, Inc.: Wallingford, CT, 2013.

4 T. Lu and F. Chen, *J. Comput. Chem.*, 2011, **33**, 580-592.

5 W. Humphrey, A. Dalke and K. Schulten, *J. Mol. Graph. Model.*, 1996, **14**, 33-38.

6 L. Yang, S. S. Saavedra and N. R. Armstrong, *Anal. Chem.*, 1996, **68**, 1834-1841.

7 X. Wang, C. Yu, H. Guo, Y. Cheng, Y. Li, D. Zheng, S. Feng and Y. Lin, *Chem. Eng. J.*, 2022, **438**, 135641.

8 M. Y. Xu, T. Wang, L. Zhou and D. B. Hua, *J. Mater. Chem. A*, 2020, **8**, 1966-1974.

9 G. H. Zhang, L. Zhang, Q. H. Zhu, H. Chen, W. L. Yuan, J. Fu, S. L. Wang, L. He and G. H. Tao, *ACS Materials Lett.*, 2021, **4**, 136-144.